

Mechanical properties of the domains of titin in a Go-like model

Marek Cieplak*

Institute of Physics, Polish Academy of Sciences, Al. Lotników 32/46, 02-668 Warsaw, Poland

Annalisa Pastore

*National Institute for Medicine Research, Department of Molecular Structure,
The Ridgeway-Mill Hill, London NW7 1AA, UK*

Trinh Xuan Hoang

Institute of Physics and Electronics, Vietnamese Academy of Science and Technology, 10 Dao Tan, Ba Dinh, Hanoi, Viet Nam

Comparison of properties of three domains of titin, I1, I27 and I28, in a simple geometry-based model shows that despite a high structural homology between their native states different domains show similar but distinguishable mechanical properties. Folding properties of the separate domains are predicted to be diversified which reflects sensitivity of the kinetics to the details of native structures. The Go-like model corresponding to the experimentally resolved native structure of the I1 domain is found to provide the biggest thermodynamic and mechanical stability compared to the other domains studied here. We analyze elastic, thermodynamic and kinetic properties of several structures corresponding to the I28 domain as obtained through homology-based modeling. We discuss the ability of the models of the I28 domain to reproduce experimental results qualitatively. A strengthening of contacts that involve hydrophobic amino acids does not affect theoretical comparisons of the domains. Tandem linkages of up to five identical or different domains unravel in a serial fashion at low temperatures. We study the nature of the intermediate state that arises in the early stages of the serial unraveling and find it to qualitatively agree with the results of Marszalek et al.

I. INTRODUCTION

The way proteins are able to sustain mechanical stress has recently attracted large interest and promoted the development of new tools, both experimental and theoretical, to study mechanical unfolding.^{1,2,3} One model system largely used for such studies is titin, a giant modular protein specific for vertebrate muscle. A single-chain titin molecule forms a filament up to $1\text{-}2\mu\text{m}$ long which connects the edge of the sarcomere, the basic unit of the muscle fibrils, with its middle (for reviews see Ref. ^{4,5,6,7}). These connections provide both a molecular ruler that determines the exact length of the sarcomere and a template for interactions with other proteins involved in muscle ultrastructure and regulation.⁷ One of the most important functions of titin is to act as a spring which confers passive elasticity on sarcomeres^{8,9,10,11,12}.

Two sequence motifs are present in the I-band, the elastic region of titin: a long stretch rich of prolines, glutamic acids, valines and lysines (PEVK motif) and up to (depending on the isoform) 100 copies of tandem bead-like globular domains whose fold belongs to the immunoglobulin (Ig) superfamily.¹³ Elasticity is thought to result from the interplay of these two elements acting as molecular springs placed in series, in which most

of the tension is provided by the largely unstructured PEVK motif, whereas the Ig domains could provide an additional contribution through a reversible unfolding mechanism.^{14,15} Most of the recent studies of titin elasticity have concentrated on the Ig element taking the 27th Ig module of cardiac titin I-band (I27) as a representative model system. Its three-dimensional structure has been determined – it is an 8 strand β sandwich with two anti-parallel β -sheets packed against each other and held together by a tight hydrophobic core.¹⁶ The N- and C-termini point to opposite directions, thus making the motif particularly suitable to a sequential assembly in a filament. Thermodynamically, I27 is highly stable both against the thermal and the chemical unfolding.^{17,18} The folding pathways both of the isolated I27 and of a homopolymer constructed by tandem I27 repeats have been characterised in detail experimentally.^{2,19,20,21} Molecular dynamics (MD) studies and other simulations have provided further details into the mechanism of unfolding suggesting that detachment of the A-strand is the earliest step in forced unfolding.^{22,23,24,25,26}

The folding, elastic, and thermodynamic properties of I27 have also been studied within the Go model.^{27,28,29} Go models^{30,31} are constructed based on the knowledge of the native structure and are coarse-grained. In their simplest version, the protein is represented by the locations of the C^α atoms. This modelling is geometry-based and is implemented by choosing effective couplings between the C^α s in a way that the ground state of the system coincides with the native conformation of the protein. This approach is less realistic than all-atom simulations but it offers many advantages. It allows one for stud-

*Correspondence to: Marek Cieplak, Institute of Physics, Polish Academy of Sciences, Al. Lotników 32/46, 02-668 Warsaw, Poland; Tel: 48-22-843-7001, Fax: 48-22-843-0926; E-mail: mc@ifpan.edu.pl

ies of: a) folding and stretching within the same model, b) tandem arrangements of many domains, c) ranges of control parameters such as temperature, T , d) more realistic pulling speeds, v_p , and e) differences and similarities between various proteins within one framework. It also highlights the link between native structure and the properties of a protein. However, it is expected that the further away from the native structure a conformation is, the more approximate the description becomes.

The focus of this paper is to consider two other Ig domains from the elastic region of titin, I1 and I28, and to compare *in silico* their mechanical, kinetic, and thermodynamic properties to those of I27 within the same theoretical framework. The three domains correspond to distinct sequences and their level of identity is low – it ranges between 30% and 40%.³²

The structure of I28 is available from homology based modelling,³² whereas the native structure of I1 has been determined experimentally by x-ray crystallography.³³ The thermodynamic stabilities of the domains have also been measured and show a remarkable difference between I1 and I27 (which are very stable) and I28 (the most unstable).¹⁷ The refolding kinetics of I28 also has been found to be about three orders of magnitude slower than that of I27.³ Despite its low thermodynamic stability, the experiments show that I28 is mechanically more stable than I27.³ Here, we produce a number of homology-based models of I28 and compare their behavior. However, in most of the paper, we focus on the model derived in.³² We show that none of the structures generates a full qualitative agreement with the experimental findings, at least when analyzed within the dynamical framework provided by a simple Go-like model.

II. SOURCE OF THE STRUCTURES USED

The experimental structures of I1 and I27 have been deposited in the Protein Data Bank³⁴ We shall refer to them hereon as I1-1g1c and I27-1tit. The I1 domain consists of 98 residues whereas I27 of 89 residues. The other two structures have been determined by homology modelling³² and will be denoted as I1-model and I28-model. I28-model was obtained using the MODELLER program.³⁵ The I1-model is the structure of a mutated sequence of I1-1g1c at a single position Gly-71-Ala. This mutation occurs in the well exposed loop region, denoted by H in the lower left panel of Figure 1, and is not expected to affect the thermodynamic or mechanical stability of the domain. It is probably an inconsequential mutation that occurs spontaneously in the system used in crystallographic studies. The root mean square deviation between this structure and the experimental I1-1g1c is about 1.16 Å. Ribbon representations of the native structures of the domains studied here are shown in Figure 1.

At the end of the paper, we shall discuss other

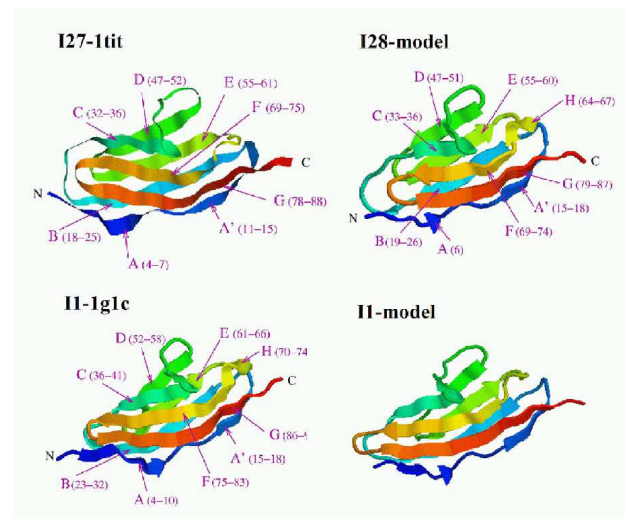


FIG. 1: The structures of the domains of titin studied in this paper. The labelling of the β -strands (symbols A through G) is indicated, together with the allocation of the amino acids to the structures. The fragments corresponding to the α -helix are denoted by H.

homology-based models of the I28 domain. These are denoted by I28-A through I28-E. I28-A and I28-B were obtained by the PSQPIR routine in the WHATIF program.³⁶ The templates used here were 1tit.pdb and 1tiu.pdb respectively – the former represents the average structure of the NMR bundle and the latter is the first structure of the NMR bundle (this structure is the best in terms of the internal energy). I28-C and I28-D used the same templates but were produced by the automatic Swissmodel webserver.³⁷ Finally, I28-E was produced by the Swissmodel webserver using the 1tlk.pdb template. The alignment, produced by clustalx,³⁸ was in any case straightforward since the sequences of I27 and I28 have the same length and do not require insertions/deletions. The sequence of telokin (1tlk) can also be structurally aligned to I27 producing a unique alignment.

III. MODEL AND METHOD

We perform molecular dynamics simulations of a continuum space Go-like model. The coarse-grained character of our theoretical description was motivated by the desire to deal with models that allow for studies of folding. The details of our approach are described in Ref.^{39,40} with refinements as presented in Ref.⁴¹. Each amino acid is represented by a point particle of mass m located at the position of the C^α atom. The interactions between amino acids are divided into native and non-native contacts. We follow a procedure given in Ref.⁴² and determine the native contacts by considering the all-atom native structure and by identifying those pairs of amino acids whose atoms effectively overlap. In the criterion of the effective overlap, the atoms are represented by spheres with

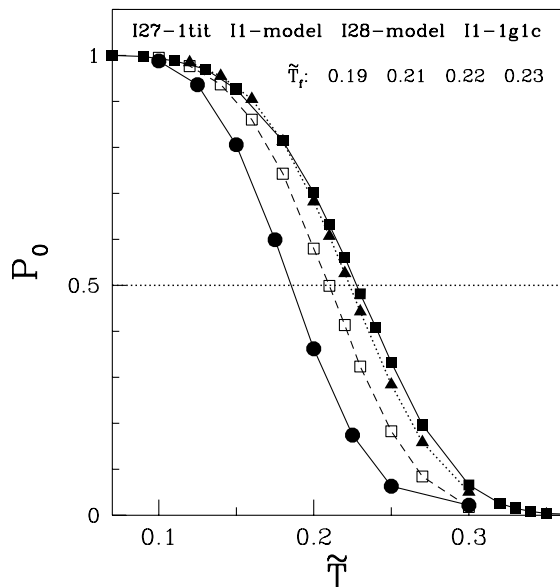


FIG. 2: Probability of staying in the native structure for the domains indicated. The lines correspond to the domains left-to-right as listed in the order at the top of the figure. The corresponding values of \tilde{T}_f are listed below in the same order.

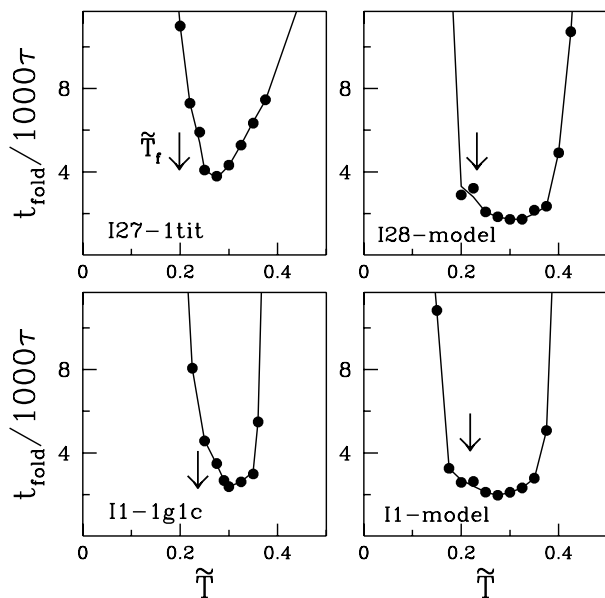


FIG. 3: Median folding times for the four systems as a function of temperature. The arrows indicate values of the folding temperature \tilde{T}_f . All of these systems are good folders in the sense that the folding temperatures are in the region of good, if not necessarily optimal, folding. The error bars are of the order of the data points (the convention kept throughout the paper).

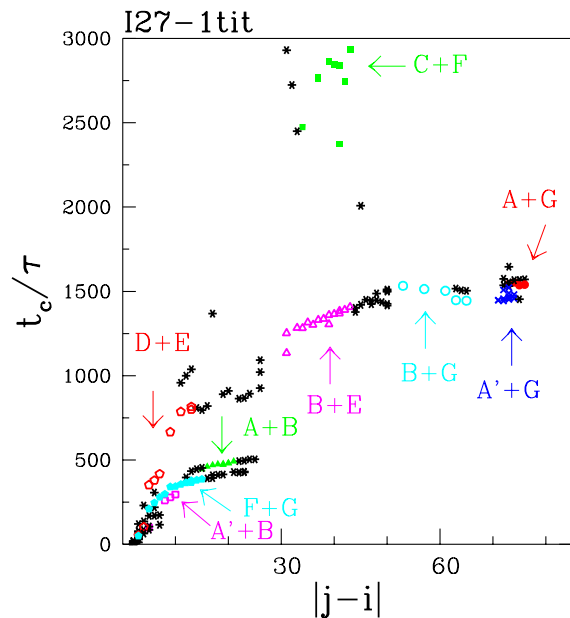


FIG. 4: The scenario of folding events for I27-1tit. The data points show average times (the average is over 200 trajectories) to establish specific contacts corresponding to the sequential distance of $|j-i|$ at the temperature of the optimal folding. The letter symbols indicate the nature of the strands that form the contacts.

radii that are a factor of 1.24 larger than the atomic van der Waals radii⁴³ to account for the softness of the potential. The native contacts are then represented by the Lennard-Jones potentials $4\epsilon[(\sigma_{ij}/r_{ij})^{12} - (\sigma_{ij}/r_{ij})^6]$, where r_{ij} is the distance between C^α atoms i and j . The length parameters σ_{ij} are determined so that the minimum of the pair potential coincides with the distance between C^α atoms in the native structure. In order to prevent entanglements, the remaining pair-wise interactions, i.e. the non-native contacts, correspond to a pure repulsion. This is accomplished by taking the Lennard-Jones potential with $\sigma_{ij} = \sigma = 5 \text{ \AA}$ and truncating it at $2^{1/6}\sigma$.

All contacts have the same energy scale ϵ . This energy scale corresponds to between 800 and 2300 K as it represents effectively hydrogen bond and hydrophobic interactions so the room temperature should correspond to $\tilde{T} = k_B T / \epsilon$ of about 0.1 – 0.3 (k_B is the Boltzmann constant). The specificity corrections could be implemented if known reliably. Replacing the Lennard-Jones potential in the contacts by a 10-12 interaction yields equivalent results both in folding⁴⁴ and in stretching.²⁹ An improved simulation might involve enhancing the strength of contacts that correspond to a disulfide bridge that is present in the I1 domain.

Neighboring C^α atoms are tethered by a harmonic potential with a minimum at 3.8 \AA and the force constant of $100\epsilon \text{ \AA}^{-2}$. A four-body term that favors the native sense of the local chirality and thus facilitates formation of local structure in a proper way is also kept in

the Hamiltonian.⁴¹ This term vanishes for the native-like chirality and introduces an energy penalty of order ϵ for the opposite chirality⁴⁵.

A Langevin thermostat with damping constant γ is coupled to each C^α to control the temperature. For the results presented below $\gamma = 2m/\tau$, where $\tau = \sqrt{m\sigma^2/\epsilon} \sim 3\text{ps}$ is the characteristic time for the Lennard-Jones potential. This produces the overdamped dynamics appropriate for proteins in a solvent,⁴¹ but is roughly 25 times smaller than the realistic damping from water,⁴⁶ Previous studies show that our choice speeds the kinetics up without altering behavior, and tests with larger γ confirm a linear scaling of folding times with γ .^{39,40} Thus the folding times reported below should be multiplied by 25 for comparison to experiment.

The stretching protocol follows the reference⁴⁷ and is implemented parallel to the initial end-to-end vector of the protein and both ends of the protein are attached to harmonic springs of spring constant k . We consider the "soft" spring case of $k = 0.12\epsilon/\text{\AA}^2$ which corresponds to typical elastic constants of AFM cantilevers. The outer end of one spring is held fixed at the origin, and the outer end of the other is pulled at constant speed v_p which results in a displacement d away from the location at the initial time. We focus on $v_p = 0.005\text{\AA}/\tau$ which corresponds to a velocity of about $7 \times 10^6 \text{ nm/s}$ when $\gamma = 2m/\tau$. Experimental AFM velocities range from 0.3 to 10 000 nm/s^{21,48,49} whereas all atom simulations correspond to speeds which are at least six orders of magnitude higher.²³ This large speed used in the all-atom simulations is believed to be one of the reasons for the peak forces that are a factor of 10 bigger than found experimentally (another, and probably more important, could be working against the surface tension of the droplet of water that surrounds the model I27 domain of titin).

The folding and stretching processes are characterized by the order in which native contacts are formed and broken respectively. The complication is that, at a finite T , a pair distance r_{ij} may fluctuate around a selected cut-off value. Thus, when discussing folding, we determine the average time t_c for each contact to form for the first time. On the other hand, when discussing stretching, we determine the average displacement, d_u , at which a contact holds for the last time. The presence of a contact between amino acids i and j is declared when r_{ij} does not exceed $1.5\sigma_{ij}$.

IV. RESULTS AND DISCUSSION

Folding of single domains of titin

Figure 2 shows the equilibrium probability, P_0 , of staying around the native state as a function of \tilde{T} . The criterion for this is that each pair that forms a native contact does not exceed the cut-off distance. P_0 depends on \tilde{T} in a sigmoidal fashion and the folding temperature, T_f , cor-

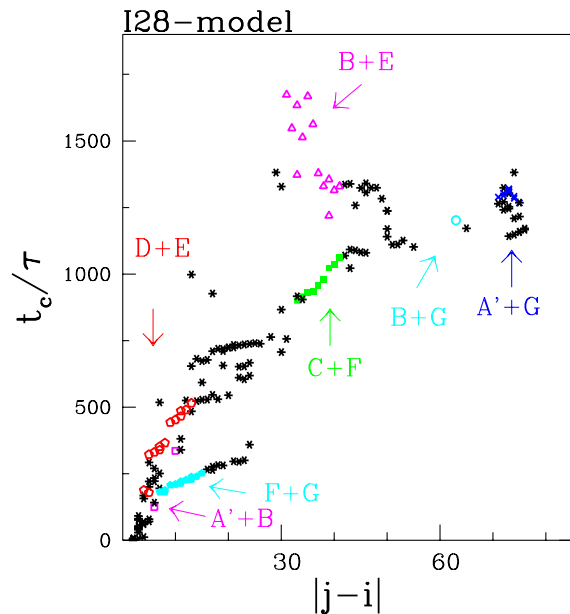


FIG. 5: Same as in Figure 4 but for I28-model.

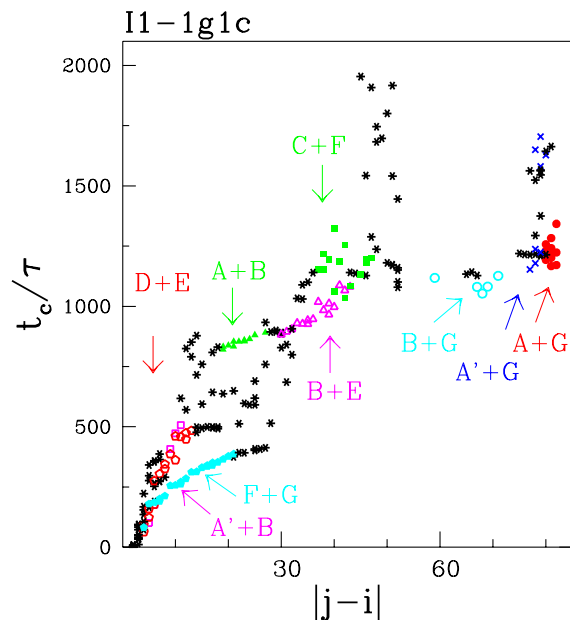


FIG. 6: Same as in Figure 4 but for I1-1g1c.

responds to P_0 crossing 0.5. The values of \tilde{T}_f do not vary much: they range between 0.19 and 0.23. The smallest value is for I27-1tit and the largest for I1-1g1c, suggesting that domain I1, at least when in isolation, should be more stable than I27. The value of \tilde{T}_f for I1-model is 0.21 – it is close to I1-1g1c but clearly the two values are not identical. I28-model appears to be more thermodynamically stable than I27 which is at variance to the experimental findings.¹⁷

In order to characterize the folding kinetics we start the system in an unfolded conformation and determine the

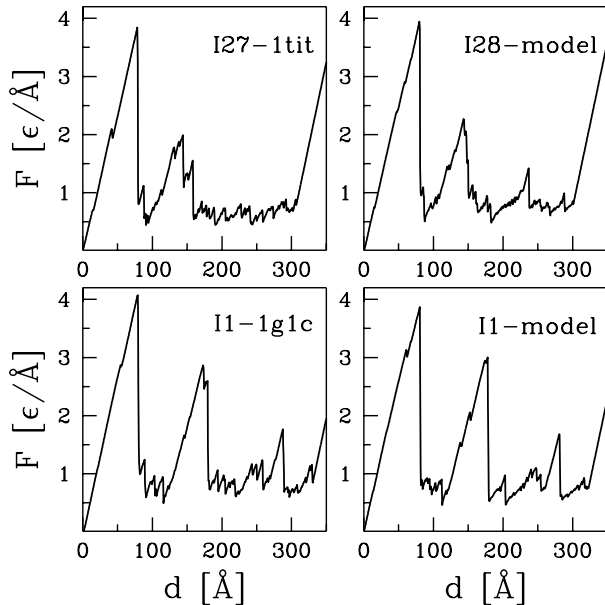


FIG. 7: Force–displacement curves for the four structures at $\tilde{T} = 0$.

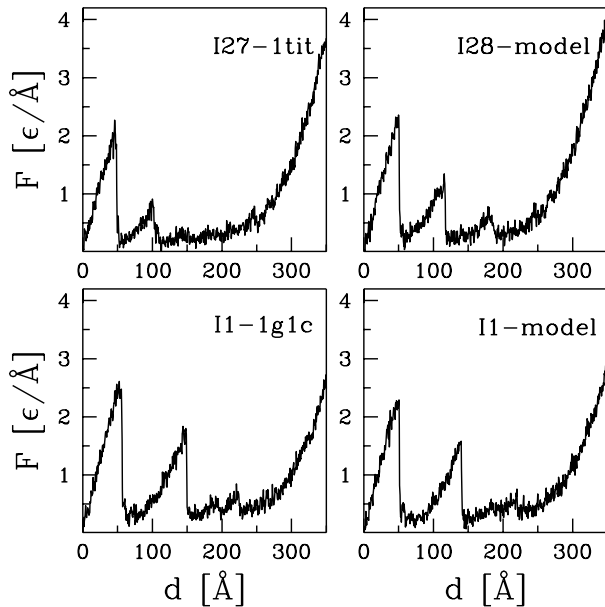


FIG. 8: Same as in Fig. 4 but for $\tilde{T}=0.3$ which should correspond to the room temperature situation. The pulling force is averaged over 100τ , i.e. over the distance of 0.5 \AA , to reduce the random noise.

median "first passage time", t_{fold} , i.e. the first time to establish all native contacts. The \tilde{T} dependence of t_{fold} is shown in Figure 3. The two homology-determined structures have a broad region of fast folding and \tilde{T}_f is within this region. On the other hand, the experimentally determined structures correspond to a significantly reduced width of the region of best folding with \tilde{T}_f being just out-

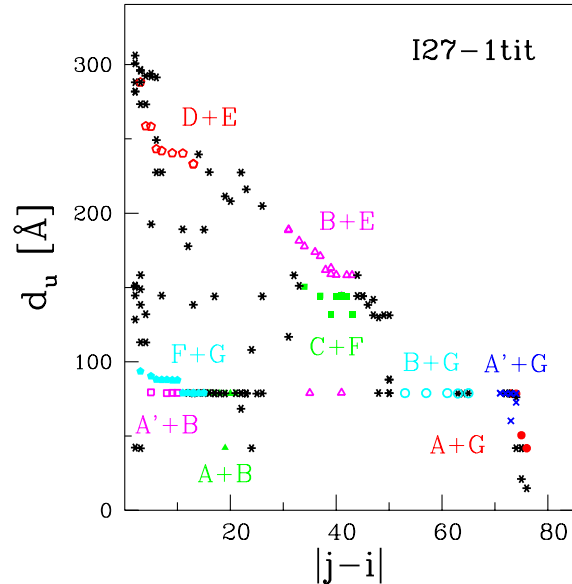


FIG. 9: The scenario of mechanical unfolding at $\tilde{T}=0$ for I27-1tit. The data points show the last distance at which particular contacts are considered to be still holding. The letter symbols are as in Figure 4.

side of this region and on the low temperature side. The optimal values of t_{fold} indicate that the structure I27-1tit is the hardest to fold to. Despite the difference in the \tilde{T} dependence between I1-model and I1-1g1c the two systems have nearly the same optimal folding times.

Figures 4 through 6 show that the four systems (results for I1-model not shown) also differ in their folding scenarios as represented by plots of t_c vs. the contact order, $|j-i|$, at the temperature of the fastest folding. I1-model shows the most monotonic dependence of t_c on $|j-i|$. However, its counterpart, I1-1g1c, concludes its folding by establishing mid-range contacts. The same happens for the remaining structures but the nature of the last contacts is specific to the structure: it is the C strand joining F in the case of I27-1tit and the B strand joining E in the case of I28-model. Each scenario involves nearly parallel branches of events taking place at various times for the same contact order. The four systems studied here are clearly not equivalent kinetically and, in particular, I1-model is not equivalent to I1-1g1c.

Stretching of single domains of titin

The dependence of the pulling force, F , on the displacement for the four structures is shown in Figures 7 and 8 for $\tilde{T}=0$ and 0.3 respectively. All of the four structures have quite similar $F-d$ patterns. The maximum force peak is large and in all cases it comes early during the unfolding providing the main resistance of the structures to the pulling device. The maximum force peak is

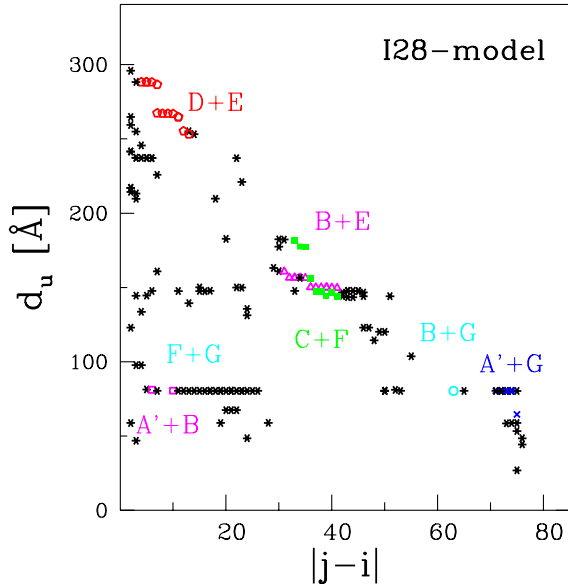


FIG. 10: Same as in Figure 9 but for I28-model.

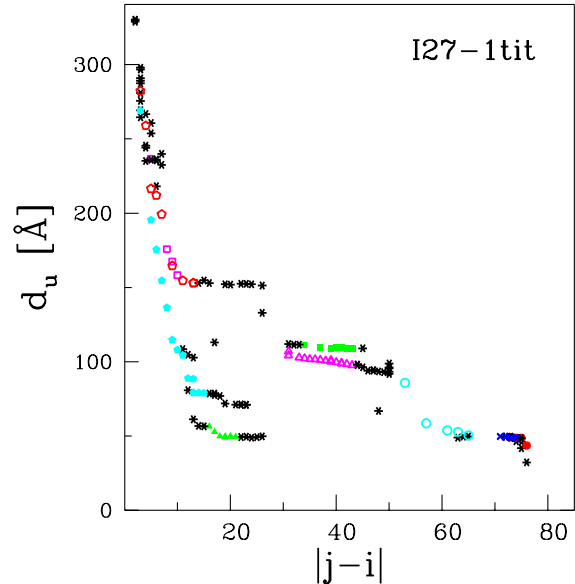
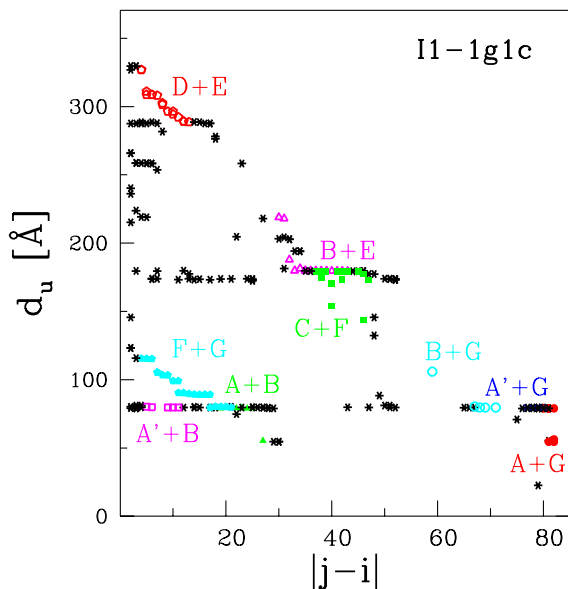
FIG. 12: Same as in Fig. 9 but for $\tilde{T}=0.3$. The data points are averaged over 20 trajectories.

FIG. 11: Same as in Figure 9 but for I1-1g1c.

the highest for I1-1g1c at both temperatures. This indicates that when standing alone I1 is the most stable domain to sustain pulling force. The heights of the maximum forces of other three structures are very close to each other. At both temperatures, I1-model appears to be mechanically less stable compared to I1-1g1c.

The second maximum in the patterns shows more variations. The details of its shape varies between the domains and its height is noticeably bigger for the two versions of the I1 domain. Unlike the first maximum, the second maximum builds up at a location which differs

somewhat from structure to structure. The third maximum is practically absent in the case of I27-1tit but it exists, in differing shapes, in the remaining three structures. The differences in the shapes and positions of the maxima are related to different sets of contacts that are involved. We note that, mechanically, I1-model appears to be nearly indistinguishable from the experimental structure I1-1g1c. Overall, the differences in the $F-d$ curves between the studied domains are subtle so the domains should be functionally equivalent in stretching.

The differences between the structures diminish as the temperature is raised and at a sufficiently high temperature, of order 0.8 in this case, the $F-d$ curves switch to a worm-like chain featureless behavior⁵⁰ in which F just grows with d monotonically combined with small thermal fluctuations.^{28,29}

The scenarios of the contact rupture at $\tilde{T}=0$ and 0.3 are shown in Figures 9 through 11 and 12 through 14 respectively. Sets of data points that form nearly horizontal lines correspond to the maxima in the $F-d$ curves. The nature of the first maximum is very similar for all of the structures studied and it involves rupturing of the A'-G contacts. The first to rupture are the strictly terminal A-G bonds but this process generates no big force. There are also varying contributions from the A'-B, A-B, B-G and F-G contacts. The second maximum involves separating strand C from F and a varying number of contacts between strand B and E. The third maximum (not present for I27-1tit) involves breaking of contacts between strands D and E.

Marszalek et al.²¹ have identified a folding intermediate in I27 - a hump on the $F-d$ curve that precedes the maximum force - as being due to the rupture

of two hydrogen bonds in A-B. This identification relies on the AFM technique combined with the steered molecular dynamics simulations and on making an amino-acidic substitution on the sixth position. Our $\tilde{T}=0$ results suggest that most of the A-B bonds (the filled triangles in Figures 9 and 12; in Figure 9 these symbols overlap with other and, except for one, are hard to see) break simultaneously with those of A'-G and one (between 4 and 23) precedes the rupture of A'-G. At $\tilde{T} = 0.3$, on the other hand, the bonds of A'-G and A-B rupture almost simultaneously. It should be noted that the coarse grained nature of the Go-like model does not allow to identify breaking of hydrogen bonds. The hydrogen bonds between the A and B strands arise probably at 5-24 and 6-24. Since we use relatively large cut-off distances for contact breaking, these contacts are still present when the 4-23 bond is ruptured. However, the relative displacement of strand A with respect to strand B should deform the hydrogen bonds. We conclude that our advance rupture of the 4-23 bond observed in the low temperature data can be related to the hydrogen bond rupture discussed in ref.²¹. Thus our results are in a qualitative agreement with the previous finding.

As the temperature is raised from $\tilde{T}=0$ to 0.3, the contact rupturing scenarios simplify somewhat: the events the contacts are more clearly grouped into several horizontal lines corresponding to the maxima in the force. For instance, the breaking of the A-G contacts at $\tilde{T}=0.3$ takes place almost at the same time as that of the A'-G bonds. The heights of the force peaks, however, decrease due to thermal fluctuations. On increasing the temperature further, the stretching scenarios become even more simplified. At $\tilde{T}=0.8$, i.e. in the entropic limit, they become strictly monotonic as a function of the contact order, as illustrated in Figure 15. In this limit, the four systems are strictly indistinguishable from the mechanic point of view.

Stretching of several domains of titin

We now generate tandem arrangements of five identical domains of titin. The $\tilde{T}=0$ $F-d$ patterns are shown in Figure 16. To a good approximation, the patterns are a serial combination of the single domain patterns of Figure 7: the proteins unwind domain by domain. The reason for this serial unwinding is that for a single domain the largest force peak is located early in the unraveling process. However, the larger the temperature, the more parallelism in the unravelling²⁸. The small shoulder before the first peak points out that all domains unfold simultaneously to a metastable state in which contacts between all terminal strands A and G and one contact (4-23) between all strands A and B break before the first domain unfolds completely. As we discussed above, this metastable state for I27 domain has been also identified as the intermediate state²¹. Note that in Ref.²¹ the authors did not consider the breaking of the A-G contacts as being an ingredient of the intermediate state. We have

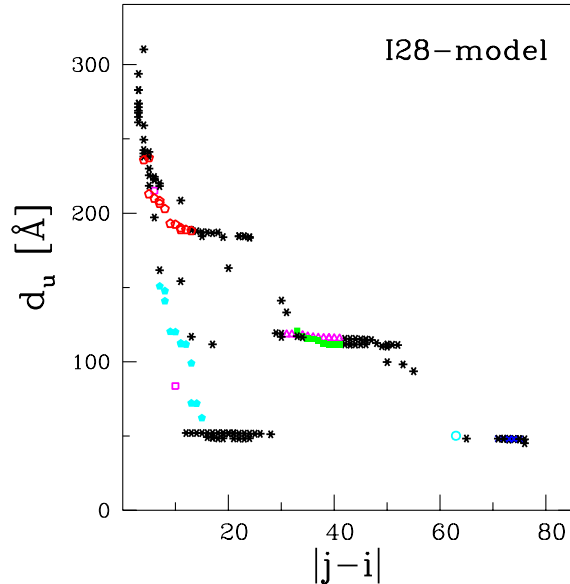


FIG. 13: The scenario of stretching for I28-model at $\tilde{T} = 0.3$.

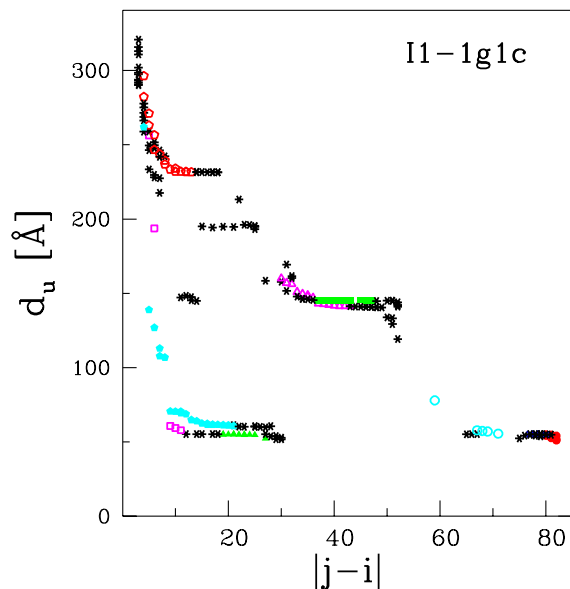


FIG. 14: The scenario of stretching for I1-1g1c at $\tilde{T} = 0.3$.

found that a similar phenomenon takes place for the two versions of the I1 domain and for I28-model. In all cases, the unfolding intermediate involves breaking of contacts between strands A and G and some contacts between strands A and B. We observe that the extension at which this happens is smaller in I1 and I28 than in I27. Figure 16 also shows that the ‘hump’ before the first peak is somewhat milder in the other domains than in I27. Note that in Ref.²¹ the ‘hump’ is also observed for a tandem arrangement of I28.

On increasing the temperature, the simultaneous un-

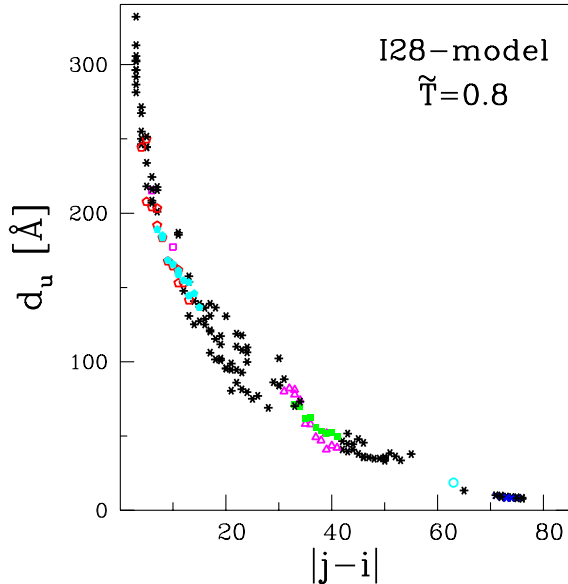


FIG. 15: The scenario of stretching for I27-1tit at $\tilde{T}=0.8$.

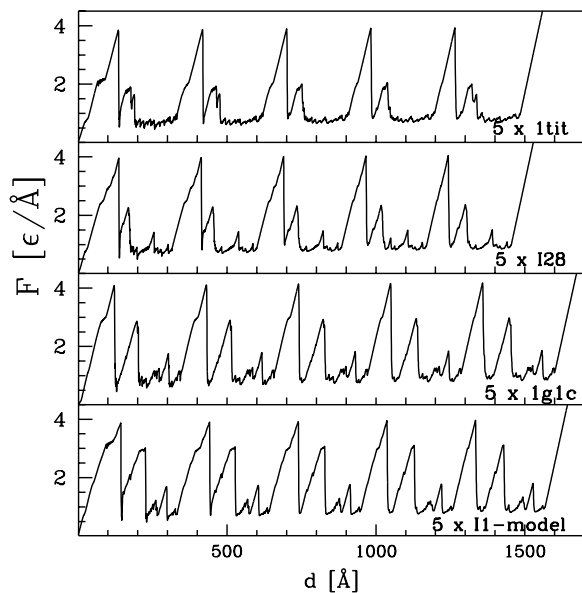


FIG. 16: Stretching of five domains of titin, linked in a tandem arrangement as listed in each panel, at $\tilde{T}=0.0$.

winding of the domains to the intermediate state still holds but also thermal fluctuations gain in importance and affect the patterns significantly. Figure 17 shows the $F-d$ patterns for various tandems of domains at \tilde{T} of 0.3. It is seen that it is only the first segment that repeats the single domain pattern fairly accurately whereas the remaining segments in the sawtooth-like pattern lose the last single domain maximum: there is no second maximum in the fivefold repeat of I27-1tit and no third maximum in the remaining fivefold repeats of the other struc-

tures. The reason for this is that the second maximum in I27-1tit and the third maximum in other structures are barely stable. As unfolding of the domains continues, thermal fluctuations (or kinetic energy) associated with the already released chain length gain in strength and destroy the peaks with low stability. Figure 17 shows that, for tandem arrangements of I28-model (the second panel) and I1-1g1c (the third panel), the second peak becomes increasingly weak. It actually disappears in the last segment of the sawtooth pattern for the case of I28-model.

It can also be seen in the top three panels of Figure 17 that the heights of the maxima in the sawtooth patterns are the highest for the I1-1g1c domains. Furthermore, the first four maxima for the I28-model domains are a bit weaker than those of I27-1tit even though they were of about the same height for the single domains. This indicates that the admixture of parallel unwinding that occurs in tandem arrangements affect mechanical stability of the individual domains. In order to study the stability differences of the domains better we have constructed heterogeneous tandem arrangements of the structures. In this case the less stable domains will unfold before the more stable ones. The two bottom panels in Figure 17 shows the $F-d$ curves for two heterogeneous tandem arrangements of five domains at $\tilde{T}=0.3$. Specifically, 3 domains of I27-1tit are linked, in an alternating fashion, with two domains of I28-model or two domains of I1-1g1c. We find that I1-1g1c is the domain that unravels the last, i.e. is the most stable. I28-model, on the other hand, shows a more complex behavior. We find that when placed in tandem with I27-1tit, I28-model is the domain that unravels the first, but after the unraveling of the first domain, the two types of domain can alternate – the order of unfolding is determined by fluctuations. This indicates that, in tandem arrangements, I28-model is only slightly less stable than I27 and the difference in mechanical stability between these two domains becomes insignificant comparing to thermal fluctuations after the first domain unfolds. This observation is consistent with the experimental findings.¹⁸ As an example, the curve shown in the last panel of Figure 17, corresponds to unraveling proceeding in the order: I28, I27, I27, I27, and I28. Figure 18 shows the snapshots of the five-domain tandem arrangements corresponding to $d=500$ Å and $\tilde{T}=0.3$ and illustrates the domain-by-domain character of the unfolding in each case.

V. SUMMARY AND CONCLUSIONS

In this paper, we have presented predictions of Go-like modeling for four native structures of titin domains and of their tandem arrangements and demonstrated that, despite noticeable differences in their native structures, the force-displacement plots and the unravelling events are qualitatively similar. Thus, the domains should be interchangeable in terms of their elastic properties. There

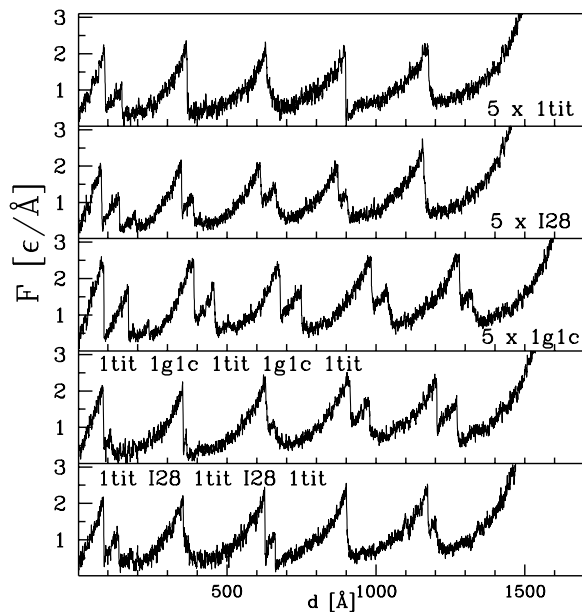


FIG. 17: Stretching of five domains of titin, linked in a tandem arrangement as listed in each panel, at $\tilde{T}=0.3$.

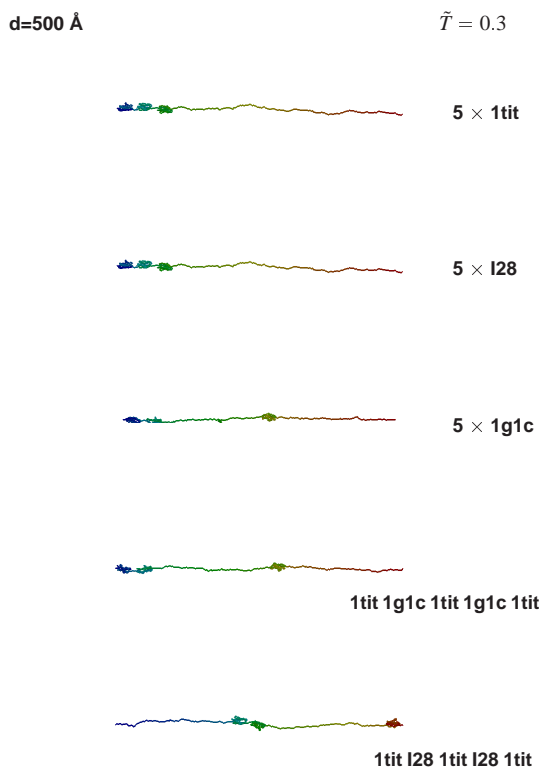


FIG. 18: Snapshots of the five-domain arrangements when stretched by 500 Å. The top-to-bottom ordering of the snapshots corresponds to the one adopted in Figure 11.

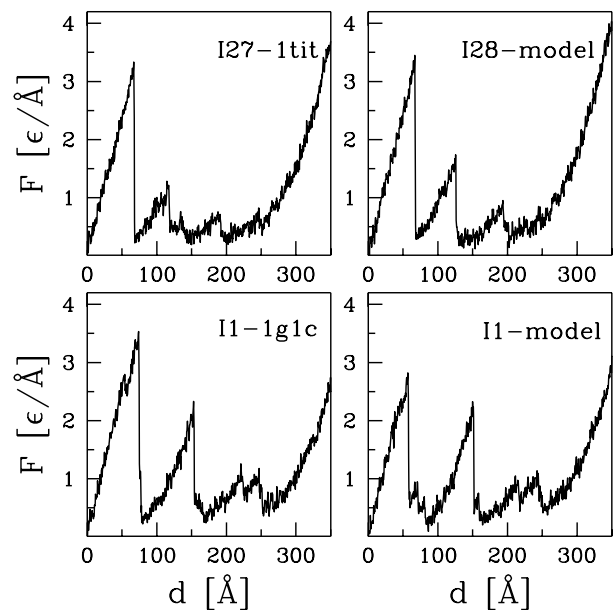


FIG. 19: An analog of Figure 6 at $\tilde{T}=0.3$ for a generalized model in which the hydrophobic-hydrophobic contacts are made stronger by a factor of two.

are also, however, substantial differences when one considers finer details of the elastic stability of the domains and their thermodynamic and kinetic properties when the domains are considered in isolation. I1-1g1c is the most stable structure in terms of its elastic resistance both separately and when placed in tandem arrangements. The I28-model domain has a mechanical stability close to that of as single domain of I27, but it is clearly less stable in tandem arrangements that involve I27.

More noticeable distinctions are observed for the thermodynamic and kinetics properties of single domains. We have shown that I1-1g1c and I28-model are the two most thermodynamically stable structures and I27-1tit is the least stable one. I28-model has a faster folding and the range of temperature in which folding is optimal is wider than I27; the same is observed for I1-model when compared to I1-1g1c. The kinetics of refolding events as studied as a function of the contact order also show clear distinctions. The contacts that form the last, on average, in the folding of I27-1tit are between strands C and F while for I28-model they are between strands B and E. In I1-1g1c and I1-model, the last events involve still other sets of contacts. Only the earliest folding events are similar in all models. All these differences show how sensitive the folding properties of the models are to the precise details of the native structures.

Most of our predictions about equivalence, or lack of it, of the domains of titin in the context of the mechanical and kinetic folding properties remains to be tested. Currently, the I27 domain has been studied experimentally in the most exhaustive way. The Go-like theoretical account of mechanical properties of I27 has turned

TABLE I: Summary of the properties of the theoretically determined structures corresponding to the I28 domain of titin as obtained within the Go model used in this paper. The first column shows a comparison to the similarly derived properties of I27-1tit. The lower the value of T_f , the lower the thermodynamic stability. The values of the Z-score listed in the table are for all contacts. They represent the deviations from the average quality value as determined by using the program WHATIF with the NEWQUA option in the QUALITY menu.

	I27-1tit	I28-model	I28-A	I28-B	I28-C	I28-D	I28-E
$F_{max} (T = 0) [\epsilon/\text{\AA}]$	3.84	3.92	3.50	3.66	4.08	3.42	3.48
\tilde{T}_f	0.185	0.224	0.174	0.172	0.192	0.178	0.214
\tilde{T}_{min}	0.275	0.30	0.25	0.275	0.25	0.275	0.275
$t_{fold}/\tau (T = T_{min})$	3700	1730	2200	2040	1800	2480	1970
$t_{fold}/\tau (T = 0.3)$	4320	1730	5440	2680	2600	2540	2060
$F_{max}^H (T = 0)^a$	4.92	5.06	4.86	4.30	4.89	4.32	4.72
Z-score	-4.85	-3.45	-6.17	-5.91	-6.10	-6.23	-3.58

^amodel with enhanced hydrophobic contacts

out to be consistent with the experimental findings.^{27,29} Some experimental results available for the I28 domain, however, appear to be at odds with our simulational results, especially when one compares I28 to I27. First of all, our studies predict the stability of I28-model to be higher than that of I27-1tit whereas the experiment shows the opposite: the melting points for I27 and I28 are 72°C and 35°C respectively.¹⁷ Secondly, our folding simulations indicate that I28-model folds faster than I27 whereas experiment shows that the folding rate of an isolated I28 domain is 0.025 s⁻¹, which is three orders of magnitude lower than that of I27 (32 s⁻¹)³ Finally, the atomic force microscopy studies³ have shown that I28 domains are mechanically more stable than I27 both in homo- and hetero-domain polyproteins whereas our studies point to nearly equivalent stabilities. This suggests that the method we are using cannot easily describe cases such as I28 whose structure is very unstable in solution. Any 'rigid' model which assumes a stable and compact structure would therefore not be appropriate to represent the experimental conditions.

One source of the discrepancy could be that our simple model incorporates just one uniform energy scale ϵ whereas a more realistic modeling would involve heterogeneous couplings. This expected lack of homogeneity might govern the subtle differences between the domains. In order to probe such effects, we have considered a generalized Go-like model in which the interactions in contacts that link two hydrophobic amino acids (ILE, LEU, MET, VAL, PHE, TRP, and TYR) are enhanced by the factor of two. Figure 19 for $\tilde{T} = 0.3$ shows that, mechanically, the relationships between the four domains in this two energy scale model are very much like as in the basic model. The noticeable difference though is that I27-1tit acquires the more pronounced third peak in the force. (The models with the two-fold enhancement of the hydrophobic-hydrophobic contact strengths are inadequate kinetically: they give rise to an easy misfolding.)

Another source of the error then may be the structure itself. The homology-based derivation of the struc-

ture may not sufficiently refined for applications that involve dynamics. Some hints can already be inferred by considering the I1 domain. Our studies show that I1-model and I1-1g1c, both meant to represent the same system, have distinct kinetics and very different stabilities: the model structure has 259 contacts instead of 288 and is less stable thermodynamically and mechanically than the experimentally derived structure. Even the force-displacement curves have distinct details indicating that a precise knowledge of the structure may affect prediction of dynamical properties in a substantial way.

We have thus generated five more homology-based structures of the I28 domains, denoted as I28-A through I28-E. I28-model and I28-E are of the highest quality, as judged from the standard structure quality checks.³⁶ The summary of their elastic, thermodynamic, and kinetic properties, as determined within our Go-model, is given in Table I and compared to those of I27-1tit. There are three conditions that should be met for a model to agree with the experimental results: 1) I28 should be more stable mechanically than I27, but 2) it should be less stable thermodynamically, and finally 3) it should refold significantly slower. An inspection of Table I indicates that none of the six I28 structures satisfies all three conditions. At best, two conditions are met in some structures. For instance, I28-C is the strongest mechanically of all of the I28 structures and it is also stronger than I27-1tit. Its folding temperature, though not lower than that of I27-1tit, is nearly to it. However, I28-C folds faster both at \tilde{T}_{min} , when folding proceeds the fastest, and at $\tilde{T}=0.3$ which appears to correspond to the room temperature. Another good choice could be I28-A. This structure yields slower folding than I27-1tit at $\tilde{T}=0.3$ and is less stable thermodynamically. However, its peak force is substantially smaller than that for I27-1tit. Incompatibly with our predictions, the Z-scores of both I28-C and I28-A are low which means that these structures are not very good in terms of packing quality. The best Z-score among the new structures has I28-E, however this structure yields

a mechanical stability which is significantly lower than that of I27-1tit.

This analysis indicates that the precise definition of the structure has a substantial impact on the predicted properties. Existence of a well defined and fairly rigid native structure is at the heart of applicability of the Go-like modeling. In the context of the I28 domain, however, this feature may also be a root of the problem given that the experimentally determined melting temperature of I28 is only 35° C. Nevertheless our analysis illustrates a possibility that using a dynamical model may augment homology-based determination of protein structures. The final message is that the simple Go-like

description can capture existence of differences in properties between various domains of titin and of their various models.

Acknowledgments

Support of M. C. from KBN in Poland (grant number 2 P03B 025 13) and from the European program IP NAPA through Warsaw University of Technology is gratefully acknowledged. T. X. H. thanks for support from the Natural Scientific Council of Viet Nam.

-
- ¹ M. Carrion-Vasquez, P. E. Marszalek, A. F. Oberhauser, and J. M. Fernandez, *Proc. Natl. Acad. Sci. USA* **96**, 11288 (1999).
- ² M. Carrion-Vazquez, A. F. Oberhauser, T. E. Fisher, P. E. Marszalek, H. Li, and J. M. Fernandez, *Prog. Biophys. Mol. Biol.* **74**, 63 (2000).
- ³ H. Li, A. F. Oberhauser, S. B. Fowler, J. Clarke, and J. M. Fernandez, *Proc. Natl. Acad. Sci. USA* **92**, 6527 (2000).
- ⁴ K. Maruyama, *Biophys. Chem.* **50**, 73 (1994).
- ⁵ K. Maruyama, *FASEB J.* **11**, 341 (1997).
- ⁶ T. C. S. Keller, *Curr. Opin. Cell Biol.* **7**, 32 (1995).
- ⁷ J. Trinick, *Curr. Biol.* **6**, 258 (1996).
- ⁸ R. Horowitz, K. Maruyama, and R. J. Podolsky, *J. Cell Biol.* **109**, 2169 (1989).
- ⁹ R. Horowitz, *Biophys. J.* **61**, 392 (1992).
- ¹⁰ T. Funatsu, et al., & S. Tsukita, *J. Cell Biol.* **120**, 711 (1993).
- ¹¹ P. H. Trombitas, W. W. Baatsen, M. S. Z. Kellermayer and G. H. Pollack *J. Cell. Sci.* **100**, 809 (1991).
- ¹² K. Wang, R. McCarter, J. Wright, J. Beverly, and R. Ramirez-Mitchell, *Proc. Natl. Acad. Sci. USA* **88**, 7101 (1991).
- ¹³ S. Labeit and B. Kolmerer, *Science* **270**, 293 (1995).
- ¹⁴ W. A. Linke, M. Ivemeyer, M. Olivieri, B. Kolmerer, C. Ruegg, and S. Labeit, *J. Mol. Biol.* **261**, 62 (1996).
- ¹⁵ W. A. Linke, and H. Granzier, *Biophys. J.* **75**, 2613 (1998).
- ¹⁶ S. Improta, A. S. Politou, and A. Pastore *Structure* **4**, 323 (1996).
- ¹⁷ A. S. Politou, D. J. Thomas, and A. Pastore, *Biophys. J.* **69**, 2601 (1995).
- ¹⁸ A. S. Politou, M. Gautel, S. Improta, L. Vangelista, and A. Pastore, *J. Mol. Biol.* **255**, 604 (1996).
- ¹⁹ S. B. Fowler, and J. Clarke, *Structure* **9**, 355 (2001).
- ²⁰ M. Carrion-Vazquez, A. F. Oberhauser, S. B. Fowler, P. E. Marszalek, S. E. Broedel, J. Clarke, and J. M. Fernandez, *Proc. Natl. Acad. Sci. USA* **96**, 3694 (1999).
- ²¹ P. E. Marszalek, H. Lu, H. B. Li, M. Carrion-Vazquez, A. F. Oberhauser, K. Schulten, and J. M. Fernandez, *Nature* **402**, 100 (1999).
- ²² R. B. Best, B. Li, A. Steward, V. Daggett, and J. Clarke, *Biophys. J.* **81**, 2344 (2001).
- ²³ H. Lu and K. Schulten, *Chem. Phys.* **247**, 141 (1999).
- ²⁴ H. Lu and K. Schulten, *Biophys. J.* **79**, 51 (2000).
- ²⁵ E. Paci and M. Karplus, *Proc. Natl. Acad. Sci. USA* **97**, 6521 (2000).
- ²⁶ D. K. Klimov and D. Thirumalai, *Proc. Natl. Acad. Sci. USA* **97**, 7254 (2000).
- ²⁷ M. Cieplak, T. X. Hoang, and M. O. Robbins, *Proteins* **49**, 114 (2002).
- ²⁸ M. Cieplak, T. X. Hoang, and M. O. Robbins, *Phys. Rev. E* **69**, 011912 (2004).
- ²⁹ M. Cieplak, T. X. Hoang, and M. O. Robbins, *Proteins: Struct. Funct. Bio.* **56**, 285 (2004).
- ³⁰ H. Abe and N. Go, *Biopolymers* **20**, 1013 (1981).
- ³¹ S. Takada *Proc. Natl. Acad. Sci. USA* **96**, 11698 (1999).
- ³² F. Fraternali and A. Pastore, *J. Mol. Biol.* **290**, 581 (1999).
- ³³ O. Mayans, J. Wuerges, M. Gautel, and M. Wilmans, *Structure* **9**, 331 (2001).
- ³⁴ F. C. Bernstein, T. F. Koetzle, G. J. B. Williams, E. F. Meyer Jr., M. D. Brice, J. R. Rodgers, O. Kennard, T. Shimanouchi, and M. Tasumi, *J. Mol. Biol.* **112**, 535 (1997).
- ³⁵ A. Sali, T. L. Blundell, *J. Mol. Biol.* **234**, 779 (1993).
- ³⁶ G. Vriend, *J. Mol. Graph.* **8**, 52 (1990).
- ³⁷ N. Guex and M. C. Peitsch *Electrophoresis* **18**, 2714 (1997).
- ³⁸ J. D. Thompson, T. J. Gibson, F. Plewniak, F. Jeanmougin, and D. G. Higgins, *Nucleic Acids Res.* **25**, 4876 (1997).
- ³⁹ T. X. Hoang, and M. Cieplak, *J. Chem. Phys.* **112**, 6851 (2000).
- ⁴⁰ T. X. Hoang, and M. Cieplak, *J. Chem. Phys.* **113**, 8319 (2001).
- ⁴¹ M. Cieplak, and T. X. Hoang, *Biophys. J.* **84**, 475 (2003).
- ⁴² M. Cieplak and T. X. Hoang, *Int. J. Mod. Phys. C* **13**, 1231 (2002).
- ⁴³ J. Tsai, R. Taylor, C. Chothia, and M. Gerstein, *J. Mol. Biol.* **290**, 253 (1999).
- ⁴⁴ M. Cieplak and T. X. Hoang, *Physica A* **330**, 195 (2003).
- ⁴⁵ J. I. Kwiecinska and M. Cieplak, *J. Phys. Cond. Mat.* (submitted).
- ⁴⁶ T. Veitshans, D. Klimov, and D. Thirumalai, *Folding Des.* **2**, 1 (1997).
- ⁴⁷ M. Cieplak, T. X. Hoang, and M. O. Robbins, *Proteins* **49**, 104 (2002).
- ⁴⁸ M. Rief, M. Gautel, F. Oesterhelt, J. M. Fernandez, and H. E. Gaub, *Science* **276**, 1109 (1997).
- ⁴⁹ S. B. Fowler, R. B. Best, J. L. Toca Herrera, T. J. Rutherford, A. Steward, E. Paci, M. Karplus M, and J. Clarke, *J. Mol. Biol.* **322**, 841 (2002).
- ⁵⁰ J. F. Marko. and E. D. Siggia, *Macromol.* **28**, 8759 (1995)